Computational Materials Science 178 (2020) 109622

Contents lists available at ScienceDirect

Computational Materials Science

journal homepage: www.elsevier.com/locate/commatsci

Ab initio simulation of amorphous BC_3

Murat Durandurdu

Department of Materials Science & Nanotechnology Engineering, Abdullah Gül University, Kayseri 38080, Turkey

ARTICLE INFO

Keywords:
Amorphous
Boron carbide
Graphite

ABSTRACT

We report the structural and electrical properties of an amorphous BC_3 model based on ab initio molecular dynamics simulations. The amorphous network is achieved from the melt and has a layer-like structure consisting of mainly hexagonal (six membered) rings as in the crystal. However, the distribution of boron atoms in the noncrystalline configuration appears to differ significantly from that of boron atoms in the crystal. The network is a solid solution and has randomly distributed nanosized graphene-like domains at each layer. Boron atoms have a tendency to form more overcoordinated defects involving with boron-boron homopolar bond(s). The mean coordination of boron and carbon atoms is 3.2 and 3.0, respectively. Interestingly the amorphous configuration is found to have a slightly higher density and bulk modulus than the crystal, which are attributed to the existence of overcoordinated units in the amorphous state. Based on the localization of the band tail states, noncrystalline BC_3 is speculated to be a semiconducting material.

1. Introduction

Graphite is the most stable crystalline form of the element carbon (C) at ambient condition and is the most explored layered crystal structure [1–3]. It presents a semimetallic character and very high chemical and heat resistances. Due to these useful properties, it has various high tech and fundamental applications. Yet in order to improve its properties and/or expand its applications, researchers have made considerable efforts to modify graphite by chemical doping [4–8], chemical functionalization [9–11] etc. Amongst these methods, the incorporation of heteroatom dopants into graphite has been shown to be an effective technique to control its properties. The replacement of C by boron (B) appears to be a naive chemical technique to alter its electrical properties [12,13].

Lowell synthesized the first solid solutions of B in graphite having up to 2.35% B content by annealing physical mixtures of graphite and boron carbide (B_4C) at temperatures up to 2500 °C [5]. Later the BC_3 compound consisting of graphite-like structure was fabricated by the interaction of boron trichloride with benzene at 800 °C [14]. The same study reported that BC_3 is a homogeneous material having a sheet-like nature but significantly turbostratic character and the layers are separated 3–4 Å apart [14]. Later experiments also revealed turbostratic or disorder nature of BC_3 [4,15,16]. At temperatures of 800–1100 °C, and using acetylene, Filipozzi et al. synthesized BC_3 and other compositions with lower B contents [17] and argued that B atoms in carbon-rich compound form B-B homopolar bonds based on magnetic resonance spectra of BC_3 and boron carbonitrides. The formation of B-B wrong bonds was also proposed for the samples synthesized at a temperature of 1140 °C [18].

Computational scientists have put great efforts to predict the staking of BC_3 layers in the bulk form using first principle calculations within different exchange correlation functionals [19–24], yet the packing of the layers still remains controversies. The AB-stacking type, as in graphite, appears to be the most stable stacking, has an orthorhombic structure with *Cmcm* symmetry [25] and shows a semiconducting behavior [25]. This layered crystal transforms to a diamond-like phase having the space group $P\bar{4}2m$ at a pressure of about 4.0 GPa based on first principles calculations [25]. The high-pressure phase of BC_3 is a superhard material with a bulk modulus of about 360 GPa and a Vickers hardness of 41 GPa [25]. In a different ab initio investigation, a transformation from *Cmcm* to *C/2C* was reported for the BC_3 crystal at 35 GPa [26] but the metallization was proposed to occur at 20 GPa. At ambient pressure the bulk modulus of *C/2C* was estimated to be 360 GPa. A transition into a monoclinic structure at about 9 GPa was recently predicted for BC_3 [27]. This phase is also a superhard material having the Vickers hardness of 43.8 GPa.

None of the phases proposed in theoretical investigations have been observed in any experiment yet. The first high pressure-experiment suggested that BC_3 transformed into a mixed state having B_4C and B-doped diamond phases at 20 GPa and 2300 K [28]. Raman studies reported the formation of diamond-like crystal at a temperature of 2033 ± 242 K and a pressure of 50 GPa [29]. The symmetry of this high-pressure phase is not known yet, to our knowledge. On the other hand, the graphite to diamond-like phase modification was not

E-mail address: murat.durandurdu@agu.edu.tr.

https://doi.org/10.1016/j.commatsci.2020.109622
Received 9 January 2020; Received in revised form 19 February 2020; Accepted 24 February 2020

observed under the shock wave loading [30]. Yet the recovered samples presented the permanent structural modifications including a local phase segregation in BC_3 and a transformation into highly disordered phases having a mixture of amorphous B_4C and graphite. Sample properties, experimental conditions/protocols etc. might be responsible for the different observations in these studies. Additional experiments are needed to better understand BC_3 at high pressure.

The existence of amorphous (disordered) phase of BC_3 (a-BC_3) might be anticipated because amorphous C with different densities exists [31]. Indeed, B doped amorphous graphite up to 25% B content can be easily fabricated experimentally [32]. Yet to our knowledge, no simulation has been carried out to explore a-BC_3 at the atomistic level. The purpose of the present work is to provide information about the short-range order of a-BC_3 and its electronic properties in details.

2. Methodology

Molecular dynamics (MD) simulations were carried out by SIESTA ab initio program [33] within a pseudopotential technique [34] and a generalized gradient approximation (GGA) [35,36]. The Γ point was used for Brillion zone integration. Double-zeta basis functions were adopted for the MD calculations. The initial configuration was a randomly distributed structure with 216 atoms (162 C atoms and 54 B atoms). The NPT approach was preferred to execute MD calculations having 1.0 fs for each time step. The starting configuration was exposed to a temperature of 5500 K for 20.0 ps and then temperature was decreased gradually to 4000 K in 5.0 ps. At this temperature the structure was equilibrated additionally for 20.0 ps and then the temperature applied was reduced to 300 K using a quenching rate of 2×10^{13} K/s. Finally, the resulting structure at 300 K was optimized using a conjugate gradient method. During the relaxation, not only the atomic positions but also the lattice parameters were relaxed. In order to compare the local structure and the electrical properties of the amorphous network with those of the crystal, the crystal having *Cmcm* symmetry and 256 atoms was contracted and its lattice parameters and atomic positions were optimized as well. The density of the relaxed amorphous and crystalline phases at ambient pressure is 1.919 g/cm^3 and 1.902 g/cm^3, respectively. So, one can see that noncrystalline state has a slightly higher density than the crystal. The physical origin of such an unusual observation will be discussed later. ISAACS [37] and VESTA [38] programs were used to get some information about the system at the atomistic level and to visualize the structures, correspondingly.

3. Results

In order to compare the atomic arrangement of the amorphous and crystalline (*Cmcm*) forms of BC_3, their partial pair correlation functions (PPCFs) are initially inspected and plotted in Fig. 1. The average B-C bond distance is positioned at 1.55 Å for the crystal and 1.54 Å for the amorphous network. The C–C bond length is located at 1.42 Å for the ordered state and 1.44 Å for the disordered one. Our values estimated for the crystal precisely overlap with the data predicted in earlier simulation [22]. From these results, one can notice a slight shortening in the B-C bond distance and a trivial enlargement in the C–C bond length by amorphization. The most drastic difference between two forms of BC_3 is observed in their B-B correlation. Specifically, the position of first two peaks of a-BC_3 is distinctively lesser than that of the crystal, indicating that the distribution of B atoms in the disordered configurations is considerably different from that of the BC_3 crystal (*Cmcm*). The first peak placed at 1.73 Å is due to B-B homopolar bonds in a-BC_3 and such bonds do not exist in the crystal but their presence was argued in turbostratic or structurally disordered BC_3[17] or high B content materials synthesized at a temperature of 1140 °C [18].

Coordination distribution of each species are provided in Table 1, which is estimated from the first minimum of PPCFs (B-B = 2.05 Å, B-C = 2.0 Å and C–C = 1.94 Å). About 95% of C atoms have sp^2 hybridization while the rest have only sp^3 hybridization. The mean coordination number of C-atoms is 3.05, parallel to 3.0 in the crystal. In the amorphous state, C–C and C–B coordination numbers are 2.18 and 0.87, respectively while they are 2.0 and 1.0 in the crystal, correspondingly. This observation advises that C atoms have a tendency to form more C–C bonds in the amorphous network than in the crystal. B atoms, on the other hand, have a coordination distribution ranging from two to five. Yet the most dominant one is sp^2 coordination with a fraction of about 78%. The average coordination number of B atoms is about 3.2, slightly higher than 3.0 in the crystal. B-C and B-B coordination numbers are 2.61 and 0.59 in the noncrystalline phase while the B-C coordination number is 3.0 for the crystal (no B-B bonds). These findings expose that the formation of overcoordinated structural defects (fourfold and fivefold) is more favorable than undercoordinated structural defects (twofold) (see Table 1) and B atoms have a trend to form more coordination defects than C atoms (see Table 1).

To offer more information about the microstructure of the amorphous network, we provide the result of the chemical environment

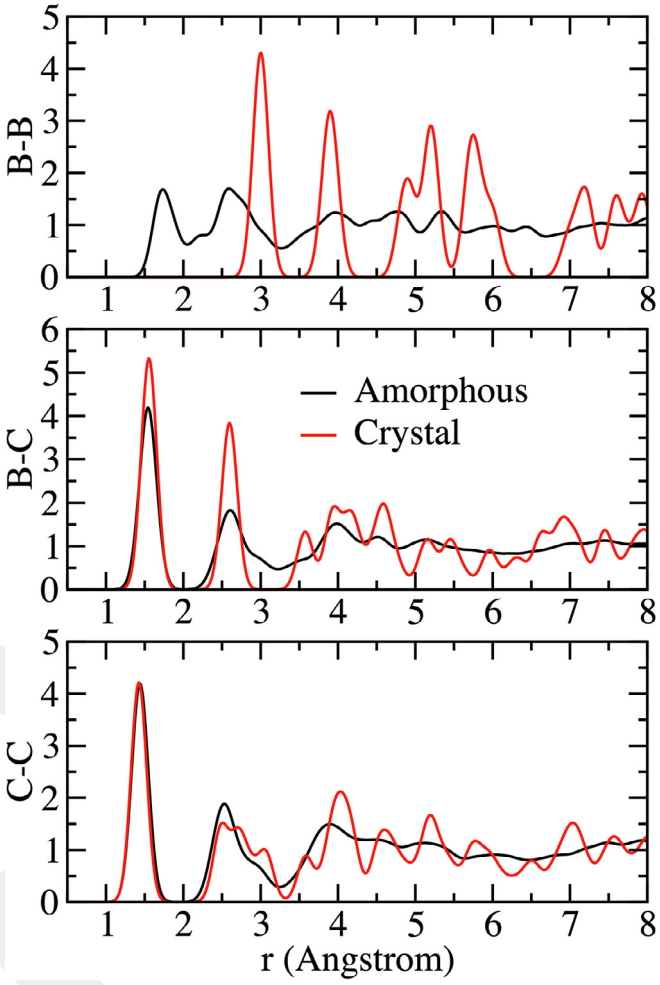

Fig. 1. Partial pair correlation functions (PPCFs) of the amorphous and crystalline phases of BC_3.

Table 1
Coordination distribution of B and C atoms in the amorphous model.

Coordination	2	3	4	5
B (%)	3.7	77.77	12.96	5.55
C (%)	0	94.44	5.55	0

Table 2
Chemical identities around B and C atoms in the amorphous configuration.

B		C	
C_3	64.815%	C_2B_1	43.210%
C_2B_1	12.963%	C_3	37.654%
C_2B_2	11.111%	C_1B_2	12.963%
C_2B_3	3.704%	C_1B_3	2.469%
C_2	3.704%	C_2B_2	1.852%
C_1B_3	1.852%	B_4	1.235%
C_1B_4	1.852%	B_3	0.617%

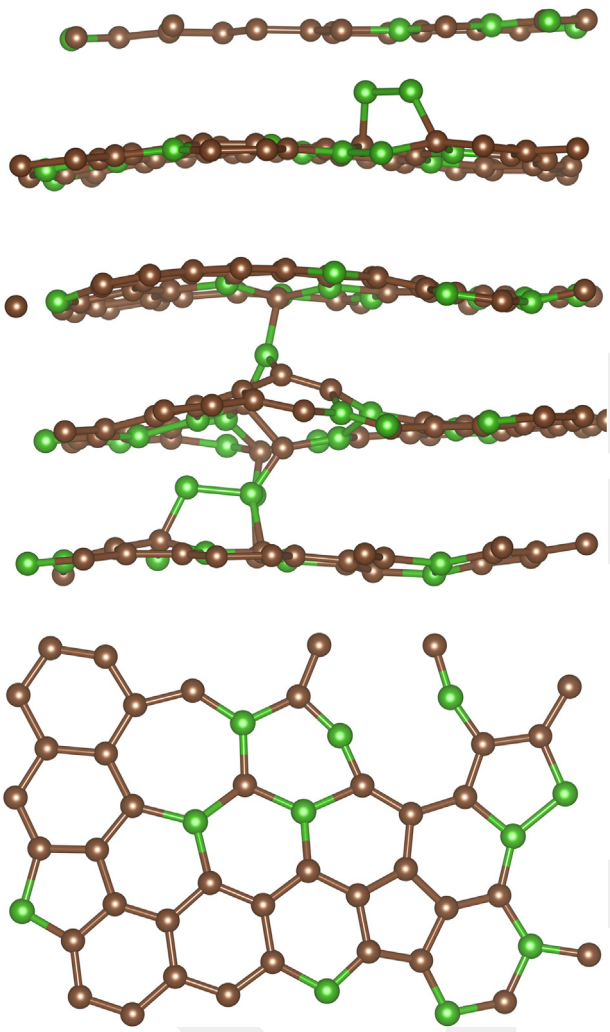

Fig. 2. Ball stick representation of a-BC_3 (top panel). A single layer extracted from the model (lower panel).

analysis in Table 2. The crystal is made of only two type motifs: B-C_3 and C-BC_2. Yet as seen in Table 2, the amorphous network presents various chemical environments for each species. C-BC_2 (~43%), C-C_3(~38%) and C-C_1B_2 (~13%) type units are the most common ones around C-atoms. Consequently, the chemical environment of about 43% of C atoms is similar that of C atoms in the crystal. The formation of C-C_3 units might denote the presence of ordered/disordered graphite-like domains in the amorphous network. A close examination of the model by visualization does indeed confirm the existence of such domains in the amorphous network (See Fig. 2). B-C_3 (~65%), B-BC_2 (~13%), B-B_2C_2 (~11%) kind configurations are the first three primary units around B atoms. Accordingly, ~65% B atoms have a chemical environment similar to that of the crystal and 11% of B atoms have a tetrahedral coordination involving with B-B homopolar bond(s).

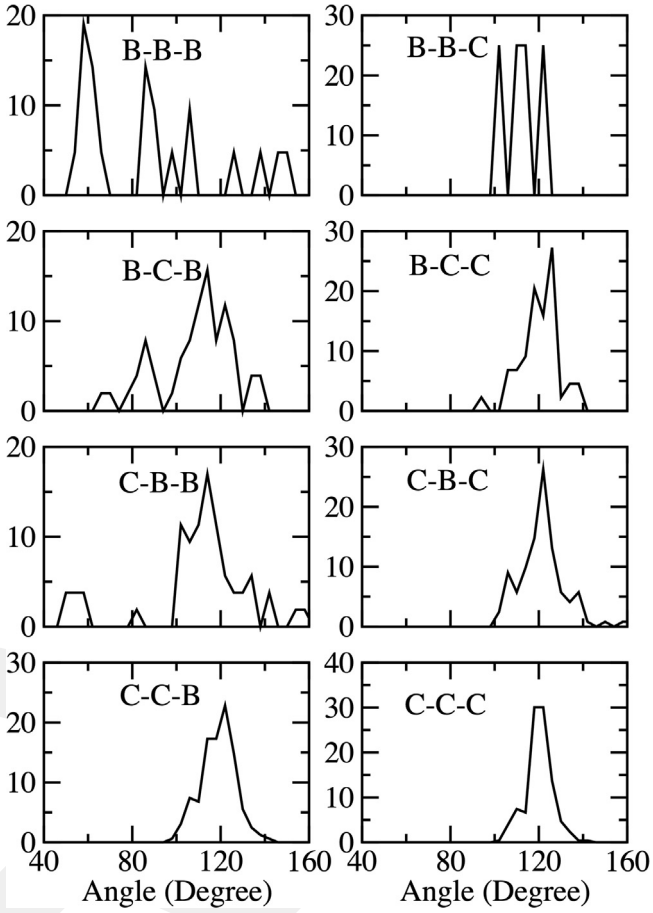

Fig. 3. Bond angle distribution functions of a-BC_3.

To deliver additional information regarding the atomic structure of the amorphous configuration, we study its bond angle distribution functions. The crystal has the B-C-C, C-B-C, C-C-B and C-C-C angles at around hexagonal angle of 120° while a-BC_3 has eight different angle distributions as shown in Fig. 3. In the amorphous form, the B-C-C, C-B-C, C-C-B and C-C-C distributions also produce a main peak around 120°, demonstrating dominant trigonal symmetry. The shoulders at below and above the hexagonal angle in these distributions are due to the five-membered and seven-membered rings, respectively as in amorphous graphite [31]. The other B-C-B, B-B-C, C-B-B and B-B-B angles present a complex and wide-angle distribution. Such large distributions are probably related to the low fraction of B-B bonds involving different membered rings.

The ring statistical analysis is executed to expose the topological connectivity of the noncrystalline network. The ring study is given in Fig. 4. The six-membered (hexagonal) rings, sole ring in the crystal, are the leading ones in the noncrystalline arrangement followed by five- and seven-membered rings. These observations are very similar to what has been proposed for amorphous graphite [31].

We reveal the electronic properties of both forms of BC_3 by analyzing their electron density of states that is provided in Fig. 5. The Fermi level is shifted to zero eV. The energy band gap of the crystal is estimated to be 0.85 eV, which is higher than 0.3 eV (Ceperly and Alder-LDA) and 0.4 eV (Perdew-Burke-Ernzerhof-GGA) values but comparable with 0.77 eV calculated using Engel–Vosko-GGA that is believed to produce better band gap energy than other GGAs [39]. The amorphous form shows no clear band gap and its EDOS is similar to that of a semimetallic material. The gap between highest occupied molecular orbital and lowest unoccupied molecular orbital is too small and about 0.14 eV. From the EDOS alone, it is hard to predict its electronic

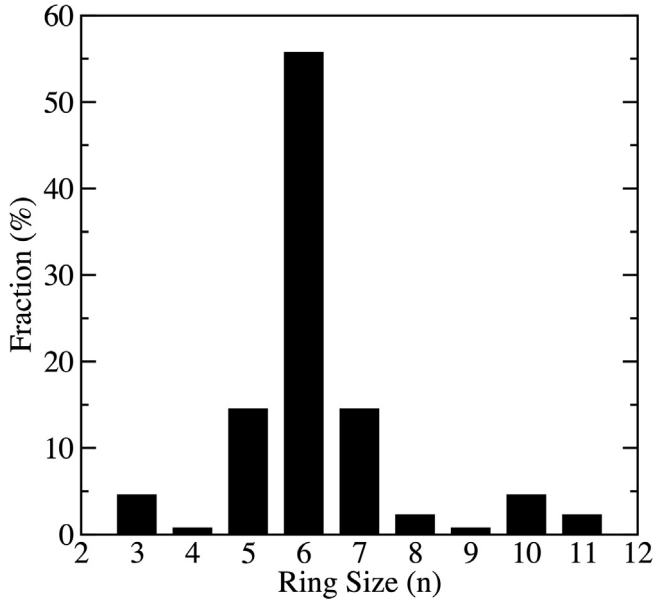

Fig. 4. Ring distribution of a-BC_3.

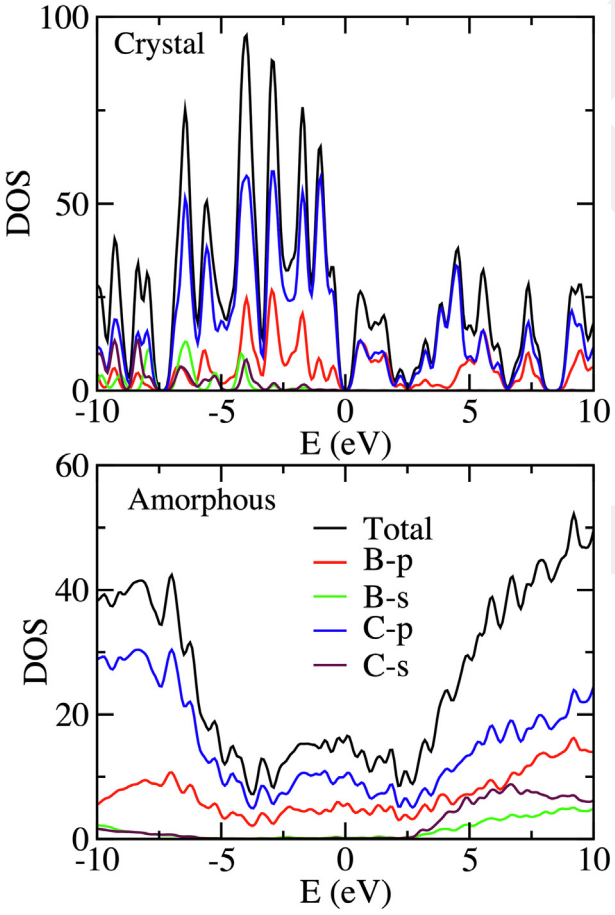

Fig. 5. Electron density of states of the amorphous and crystalline phases of BC_3.

nature without any hesitation. Therefore, we study the localization of the band tail states of a-BC_3 by using *inverse participation ratio* (IPR)

$$IPR(\psi_j) = N \sum_{i=1}^{N} a_i^{m4} / (\sum_{i=1}^{N} a_i^{m2})^2$$

where $\psi_m = \sum_{i=1}^{N} a_i^m \phi_i$ is the m^{th} eigenstate and N corresponds to the

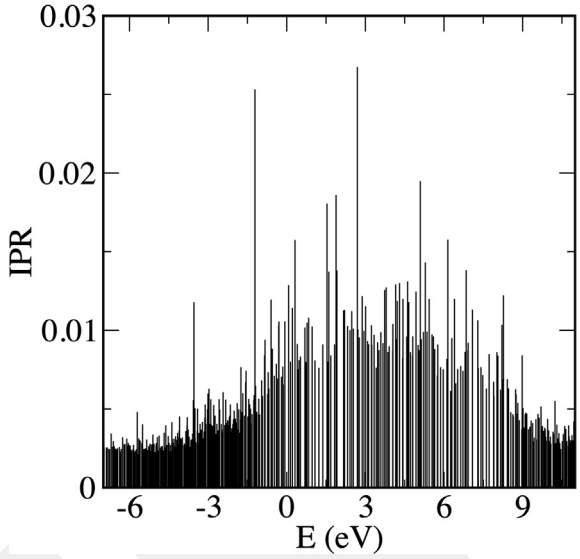

Fig. 6. Inverse participation ratio (IPR) of a-BC_3.

number of atoms. The IPR estimated for the amorphous model is offered in Fig. 6. One can see that both valance and conduction states around the Fermi level (at zero eV) are rather localized due to their high IPR values. By considering underestimation of band gap energy in DFT-GGA calculations, the localized tail states (the states are extended for metallic systems) and the experimental observation of a metal-to-insulator phase changed in B-doped amorphous graphite depending on B content [32], we speculate that a-BC_3 is a semiconducting material, albeit with small band gap energy. Yet experimental works or hybrid exchange functional calculations are necessary to reveal the true electronic behavior of a-BC_3. To offer further understanding about the electronic structure of the BC_3 forms, we evaluate the partial electron density of states as well. It appears that C-p states have main impact on both valence and conduction bands near the Fermi energy. B-p states also have some influence to them.

In order to calculate the relative energy difference between the ordered and disordered phases and their equilibrium volume and bulk modulus, their energy-volume relation (see Fig. 7) is estimated using a variable cell optimization technique and fitted to the third-order Birch-Murnaghan equation of state

$$E(V) = E_0 + \frac{9V_0K}{16}\left\{\left[\left(\frac{V_0}{V}\right)^{\frac{2}{3}} - 1\right]^3 K' + \left[\left(\frac{V_0}{V}\right)^{\frac{2}{3}} - 1\right]^2 \left[6 - 4\left(\frac{V_0}{V}\right)^{\frac{2}{3}}\right]\right\}$$

The equilibrium volume (V_0) is estimated to be 10.155 $Å^3$/atom for the amorphous model and to be 10.22 $Å^3$/atom for the crystal. Accordingly, the amorphous phase has a slightly lower volume than the crystal. Their relative energy difference at the equilibrium is 0.15 eV/atom. From the equation of state, the bulk modulus is proposed to be about 24 GPa for the crystalline structure and 35 GPa for the non-crystalline configuration. Subsequently, an increase in the bulk modulus of BC_3 is experienced by amorphization.

4. Discussion

The structural analyses reveal that a-BC_3 has a layered structure as in the crystal and some layers are linked each other by B-atoms as seen in Fig. 2. The connectivity of network is similar to amorphous graphite [31]. The local structure of a-BC_3, however, is different from that of the crystal. Specifically, the distribution of B atoms in the amorphous network is not analogous to that of B atoms in the crystal. Such a different distribution produces unsystematically dispersed nanosized graphene-like domains at each layer. Overcoordinated defects, in

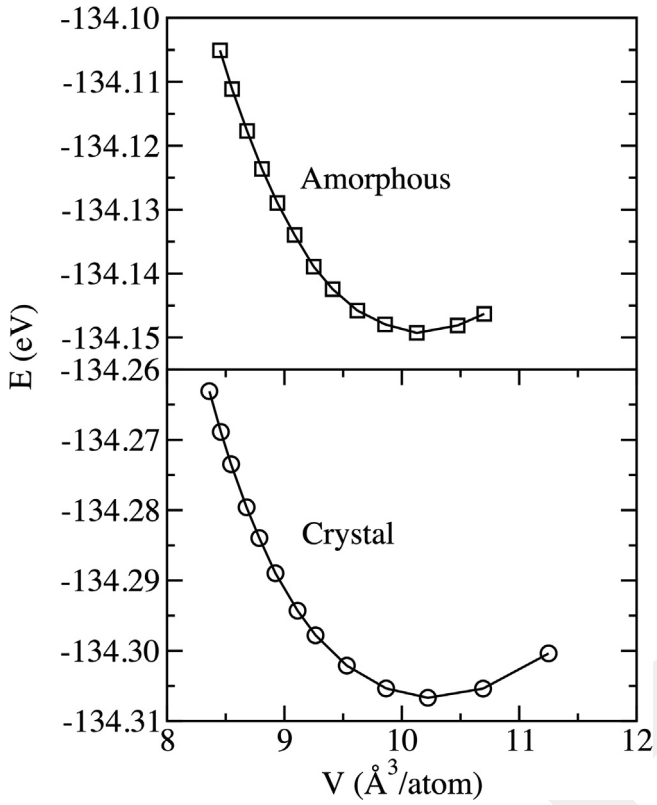

Fig. 7. Energy-volume relation of the amorphous and crystalline phases of BC_3.

particular sp^3 bonds, and chemical defect (the formation of B-B homopolar bonds) are two other essential differences between the amorphous and crystalline structures. Considering the occurrence of B-B bonds in some samples having high B content (~25%)[17,18], the observation of such bonds in a-BC_3 might be unsurprising. This result might imply that a-BC_3 is structurally closer to the turbostratic BC_3 than to the crystal.

In a contrast to what has been observed in most amorphous materials in which amorphization leads to a lower density, a-BC_3 has a slightly higher density and bulk modulus than the crystal. This is attributed to the formation of sp^3 motifs and linkages between some layers provided by B atoms.

Our disordered network appears to be different from the one formed under shock compression experiment [30]. A mixture of amorphous B_4C and graphite is not witnessed but a solid solution is perceived in the present study. This observation is especially important because it suggests that amorphous phase of BC_3 having a significantly diverse local structure can be fabricated depending on preparation protocols and might have distinctive physical, electrical, mechanical and chemical properties. Consequently a-BC_3 might offer a wide range of high-tech applications. Therefore, additional studies using different experimental conditions or procedures (temperature, nonhydrostatic compression, irritation, etc.) are necessary to reveal its properties and potential applications.

5. Conclusions

The atomic structure and electrical features of an amorphous BC_3 model are discussed based on ab initio MD calculations. The model is generated using “melt and quench” technique and has a layer-like structure as in the crystal. The connectivity of the network is mainly due to hexagonal (six membered) rings, similar to the crystal, but the distribution of B atoms in the amorphous structure seems to differ considerably from that of B atoms in the crystal. The distribution of B atoms yields arbitrarily dispersed nanosized graphene-like domains. B atoms involve more overcoordinated defects having B-B homopolar bond(s) and its mean coordination is 3.2. The presence of higher coordinated motifs in the amorphous state leads to a marginally higher density and bulk modulus than the crystal. The localization of the band tail states is perceived and hence noncrystalline BC_3 is proposed to be a semiconducting material. All conclusions are based on a 216-atom amorphous model. We believe that this model provides accurate information about the short-range order but the medium range order cannot be captured due to its small size. For larger systems, the size of graphene-like domains or well separated domains will be more visible and a clear picture about the medium range order and phase separations if any can be easily attainable. Therefore, additional theoretical studies on larger systems are more desirable to probe its microstructure in details.

Declaration of Competing Interest

The authors declare that they have no known competing financial interests or personal relationships that could have appeared to influence the work reported in this paper.

Acknowledgements

This work was supported by the Abdullah Gül University Support Foundation. The simulations were partially run on the TÜBİTAK ULAKBİM, High Performance and Grid Computing Center (TRUBA resources).

Data availability

The raw/processed data required to reproduce these findings cannot be shared at this time as the data also forms part of an ongoing study.

Appendix A. Supplementary data

Supplementary data to this article can be found online at https://doi.org/10.1016/j.commatsci.2020.109622.

References

[1] R. Sengupta, M. Bhattacharya, S. Bandyopadhyay, A.K. Bhowmick, A review on the mechanical and electrical properties of graphite and modified graphite reinforced polymer composites, Prog. Polym. Sci. 36 (2011) 638–670.
[2] S.C. Chelgani, M. Rudolph, R. Kratzsch, D. Sandmann, J. Gutzmer, A review of graphite beneficiation techniques, Min. Proc. Ext. Met. Rev. 37 (2016) 58–68.
[3] D.D. Chung, Review graphite, J. Mater. Sci. 37 (2002) 1475–1489.
[4] N.P. Stadie, E. Billeter, L. Piveteau, K.V. Kravchyk, M. Döbeli, M.V. Kovalenko, Direct synthesis of bulk boron-doped graphitic carbon, Chem. Mater. 29 (2017) 3211–3218.
[5] C.E. Lowell, Solid solution of boron in graphite, J. Am. Ceram. Soc. 50 (1967) 142–144.
[6] T. Hagio, M. Nakamizo, K. Kobayashi, Studies on X-ray diffraction and Raman spectra of B-doped natural graphite, Carbon 2 (1989) 259–263.
[7] T. Shirasaki, A. Derré, M. Ménétrier, A. Tressaud, S. Flandrois, Synthesis and characterization of boron-substituted carbons, Carbon 10 (2000) 1461–1467.
[8] J.S. Burgess, C.K. Acharya, J. Lizarazo, N. Yancey, B. Flowers, G. Kwon, et al., Boron-doped carbon powders formed at 1000 C and one atmosphere, Carbon 13 (2008) 1711–1717.
[9] Y.L. Zhong, T.M. Swager, Enhanced electrochemical expansion of graphite for in situ electrochemical functionalization, J. Am. Ceram. Soc. 134 (2012) 17896–17899.
[10] Z. Yang, Y. Sun, L.B. Alemany, T.N. Narayanan, W.E. Billups, Birch reduction of graphite. Edge and interior functionalization by hydrogen, J. Am. Chem. Soc. 134 (2012) 18689–18694.
[11] S. Aliyeva, R. Alosmanov, I. Buniyatzadeh, A. Azizov, A. Maharramov, Recent developments in edge-selective functionalization of surface of graphite and derivatives–a review, Soft Mater. 17 (2019) 1–9.
[12] M. Endo, C. Kim, T. Karaki, Y. Nishimura, M.J. Matthews, S.D.M. Brown, et al., Anode performance of a Li ion battery based on graphitized and B-doped milled mesophase pitch- based carbon fibers, Carbon 37 (1999) 561–568.
[13] M. Endo, T. Hayashi, S.H. Hong, T. Enoki, M.S. Dresselhaus, Scanning tunneling microscope study of boron-doped highly oriented pyrolytic graphite, J. Appl. Phys.

90 (2001) 5670–5674.
[14] J. Kouvetakis, R.B. Kaner, M.L. Sattler, N. Bartlett, A novel graphite-like material of composition BC_3, and nitrogen-carbon graphites, J. Chem. Soc., Chem. Commun. 24 (1986) 1758–1759.
[15] T.C. King, P.D. Matthews, H. Glass, J.A. Cormack, J.P. Holgado, M. Leskes, J.M. Griffin, et al., Theory and practice: bulk synthesis of C3B and its H2-and Li-storage capacity, Angew. Chem. Int. Ed. 54 (2015) 5919–5923.
[16] O.O. Kurakevych, T. Chauveau, V.L. Solozhenko, On crystal lattice parameters of graphite-like phases of the BC system, J. Superhard Mater. 32 (2010) 231–235.
[17] L. Filipozzi, A. Derré, J. Conard, L. Piraux, A. Marchand, Local order and electrical properties of boron carbonitride films, Carbon 33 (1995) 1747–1757.
[18] T. Shirasaki, A. Derré, M. Ménétrier, A. Tressaud, S. Flandrois, Synthesis and characterization of boron-substituted carbons, Carbon 38 (2000) 1461–1467.
[19] R. Magri, Ordering in B x C 1–x compounds with the graphite structure, Phys. Rev. B 49 (1994) 2805–2815.
[20] Q. Wang, Long-Qing Chen, J.F. Annett, Stability and charge transfer of C 3 B ordered structures, Phys. Rev. B 54 (1996) R2271–R2275.
[21] Q. Wang, J.F. Long-Qing Chen, Ab Annett, initio calculation of structural properties of C 3 B and C 5 B compounds, Phys. Rev. B 55 (1997) 8–10.
[22] D. Tomanek, R.M. Wentzcovitch, S.G. Louie, M.L. Cohen, Calculation of electronic and structural properties of BC 3, Phys. Rev. B 37 (1988) 3134–3136.
[23] H. Sun, F.J. Ribeiro, D. Je-Luen Li, M.L. Roundy, S.G. Cohen, Ab Louie, initio pseudopotential studies of equilibrium lattice structures and phonon modes of bulk BC 3, Phys. Rev. B 69 (2004) 024110–024119.
[24] B. Ozdemir, V. Barone, Structural and electronic properties of crystalline graphite-like BC3, Comp. Mater. Sci. 109 (2015) 248–252.
[25] Z. Liu, J. He, J. Yang, X. Guo, H. Sun, H.T. Wang, et al., Prediction of a sandwich like conducting superhard boron carbide: First-principles calculations, Phys. Rev. B 73 (2006) 172101–172104.
[26] Z. Jin-Ling, C. Tian, M. Yan-Ming, L. Zhi-Ming, L. Bing-Bing, Z. Guang-Tian, Effects of high pressure on BC3, Chin. Phys. Lett. 23 (2006) 2538–2541.
[27] Mengdong Ma, B. Yang, Z. Li, M. Hu, Q. Wang, L. Cui, D. Yu, J. He, A metallic superhard boron carbide: first-principles calculations, Phys. Chem. Chem. Phys. 17 (2015) 9748–9751.
[28] V.L. Solozhenko, N.A. Dubrovinskaia, L.S. Dubrovinsky, Synthesis of bulk superhard semiconducting B-C material, Appl. Phys. Lett. 85 (2004) 1508–1510.
[29] P.V. Zinin, L.C. Ming, I. Kudryashov, N. Konishi, S.K. Sharma, Raman spectroscopy of the BC3 phase obtained under high pressure and high temperature, J. Raman Spectrosc. 38 (2007) 1362–1367.
[30] T. De Rességuier, O.O. Kurakevych, A. Chabot, J.P. Petitet, V.L. Solozhenko, Structural changes and phase stability of graphitelike BC 3 under explosive shock-wave loading, J. Appl. Phys. 108 (2010) 083522.
[31] B. Bhattarai, D.A. Drabold, Amorphous carbon at low densities: An ab initio study, Carbon 115 (2017) 532–538.
[32] P.N. Vishwakarma, S.V. Subramanyam, Metal–insulator transition in boron-doped amorphous carbon films, Philos. Mag. 87 (2007) 811–821.
[33] P. Ordejón, E. Artacho, J.M. Soler, Self-consistent order-N density- functional calculations for very large systems, Phys. Rev. B 53 (1996) R10441–R10444.
[34] N. Troullier, J.L. Martins, Efficient pseudopo tentials for plane-wave calculations, Phys. Rev. B 43 (1991) 1993–2006.
[35] A.D. Becke, Density functional exchange energy approximation with correct asymptotic behavior, Phys. Rev. A 38 (1988) 3098–3100.
[36] C. Lee, W. Yang, R.G. Parr, Development of the Colle-Salvetti correlation-energy formula into a functional of the electron density, Phys. Rev. B 37 (1988) 37785–37789.
[37] S. Le Roux, V. Petkov, ISAACS–interactive structure analysis of amorphous and crystalline systems, J. Appl. Crystallogr. 43 (2010) 181–185.
[38] K. Momma, F. Izumi, VESTA 3 for three-dimensional visualization of crystal, volumetric and morphology data, J. Appl. Crystallogr. 44 (2011) 1272–1276.
[39] A.H. Reshak, Specific features of electronic structures and optical susceptibilities of g-BC 3 and t-BC3 phases, Phys. Chem. Chem. Phys. 17 (2015) 8006–8016.